Geophysical Research Letters

RESEARCH LETTER
10.1029/2023GL107930

# How Volcanic Aerosols Globally Inhibit Precipitation

Zachary McGraw[1,2] and Lorenzo M. Polvani[1,3,4]

[1]Department of Applied Physics and Applied Mathematics, Columbia University, New York, NY, USA, [2]NASA Goddard Institute for Space Studies, New York, NY, USA, [3]Department of Earth and Environmental Sciences, Columbia University, New York, NY, USA, [4]Lamont-Doherty Earth Observatory, Columbia University, Palisades, NY, USA

**Key Points:**

- We identify the mechanisms of volcanic aerosol influence on global precipitation by assessing the atmospheric energy budget in simulations
- Post-eruption precipitation reduction is largely a consequence of a cooler surface, with latent heat balancing a less emissive troposphere
- Volcanic aerosols absorb outgoing longwave radiation into the stratosphere, and the added energy causes additional precipitation reduction

**Supporting Information:**

Supporting Information may be found in the online version of this article.

**Correspondence to:**

Z. McGraw,
zachary.mcgraw@columbia.edu

**Citation:**

McGraw, Z., & Polvani, L. M. (2024). How volcanic acrosols globally inhibit precipitation. *Geophysical Research Letters*, *51*, e2023GL107930. https://doi.org/10.1029/2023GL107930

Received 19 DEC 2023
Accepted 9 MAY 2024

**Author Contributions:**

**Conceptualization:** Zachary McGraw, Lorenzo M. Polvani
**Formal analysis:** Zachary McGraw
**Funding acquisition:** Lorenzo M. Polvani
**Investigation:** Zachary McGraw, Lorenzo M. Polvani
**Methodology:** Zachary McGraw, Lorenzo M. Polvani
**Project administration:** Lorenzo M. Polvani
**Resources:** Zachary McGraw, Lorenzo M. Polvani
**Supervision:** Lorenzo M. Polvani
**Visualization:** Zachary McGraw



**Abstract** Volcanic aerosols reduce global mean precipitation in the years after major eruptions, yet the mechanisms that produce this response have not been rigorously identified. Volcanic aerosols alter the atmosphere's energy balance, with precipitation changes being one pathway by which the atmosphere acts to return toward equilibrium. By examining the atmosphere's energy budget in climate model simulations using radiative kernels, we explain the global precipitation reduction as largely a consequence of Earth's surface cooling in response to volcanic aerosols reflecting incoming sunlight. These aerosols also directly add energy to the atmosphere by absorbing outgoing longwave radiation, which is a major cause of precipitation decline in the first post-eruption year. We additionally identify factors limiting the post-eruption precipitation decline, and provide evidence that our results are robust across climate models.

**Plain Language Summary** Large volcanic eruptions can emit gas into the stratosphere that chemically forms sulfate aerosol particles. These aerosols persist in the stratosphere for up to 2 years, and have been linked to widespread precipitation changes in studies based on observations and models. Here we identify the mechanisms through which volcanic aerosols cause their clearest precipitation impact, a temporary reduction in global mean precipitation. Volcanic aerosols globally inhibit precipitation as a result of their abilities to both reflect incoming solar radiation and absorb longwave (terrestrial) radiation. The first is the more important influence on global precipitation, which is reduced for several years as an energetic response to cooler tropospheric temperatures. Absorption of longwave radiation further reduces precipitation during the first post-eruption year, as a response to the increased energy brought into the stratosphere.

## 1. Introduction

Stratospheric aerosols from volcanic eruptions have been linked to widespread disruptions in precipitation observed during the 20th century, most notably a decline in global mean precipitation following the 1991 eruption of Mt. Pinatubo (Adler et al., 2018; Gillett et al., 2004). Global impacts of volcanic eruptions are important to evaluate given potential influences on societies and ecosystems and implications for stratospheric aerosol geoengineering (Proctor et al., 2018; Trenberth & Dai, 2007). While climate models indicate that volcanic aerosols reduce global mean precipitation in the years following eruptions (Iles & Hegerl, 2014; Robock & Liu, 1994), little has been done to understand the underlying mechanisms. This contrasts with efforts to understand regional post-eruption precipitation changes associated with monsoons (Liu et al., 2016; Zhuo et al., 2020) and the intertropical convergence zone (Colose et al., 2016). In this study we identify how precipitation is globally reduced as a consequence of volcanic aerosol presence in the stratosphere.

The atmospheric energy budget is essential for elucidating the mechanisms by which volcanic aerosols alter precipitation, as precipitation reflects the amount of latent heat cycled into the atmosphere through condensation. A perturbation to the climate system initiates a multitude of changes to the atmosphere's energy budget, including radiative, sensible, and latent energy responses. The atmospheric energy budget then tends toward a new equilibrium, with the sum of all energy flux changes close to zero. The precipitation response may be represented as equal to the sum of balancing terms (O'Gorman et al., 2012):

$$L\Delta P \approx \underbrace{-\Delta R_{ATM} - \Delta SH}_{\Delta Q} - \Delta H \tag{1}$$

Here $\Delta P$ is the precipitation anomaly and $L$ is the latent heat of condensation constant. The atmospheric radiative flux anomaly $\Delta R_{ATM} = \Delta R_{TOA} - \Delta R_{SFC}$, is the difference in radiative flux anomalies between the

**Writing – original draft:** Zachary McGraw
**Writing – review & editing:** Zachary McGraw, Lorenzo M. Polvani

top-of-atmosphere and surface, and $\Delta SH$ is surface-to-atmosphere sensible heat flux anomaly. $\Delta R_{ATM}$ includes the immediate influence of aerosol-radiation interactions on the net energy flux into the atmosphere (hereafter $\Delta R_{ATM,IRF}$, where IRF is instantaneous radiative forcing, or the atmospheric *aerosol forcing* for short), plus radiative flux responses as the Earth-climate system adjusts to the aerosol presence. $\Delta H$ is horizontal transport of dry static energy, which includes circulation responses. $\Delta H$ can be neglected at length scales of at least several thousand kilometers (Dagan & Stier, 2020; O'Gorman et al., 2012), and since global mean precipitation is our focus we mostly do so here. The equality in Equation 1 is approximate (≈) because the atmosphere takes time to fully adjust to the stratospheric aerosol layer, which continuously evolves. To simplify our analysis, we define $\Delta Q = -\Delta R_{ATM} - \Delta SH$, the diabatic cooling excluding latent heat (or *diabatic cooling* for short), as in O'Gorman et al. (2012).

Atmospheric energy responses to a given forcing (e.g., greenhouse gases or volcanic aerosols) are most often decomposed into *rapid adjustments* (RA) and *sea surface temperature* (SST) *mediated responses*. The rapid adjustments are atmospheric energy changes other than the IRF that would occur without SSTs responding to the forcing. When evaluating climate sensitivity the SST-mediated responses are usually discussed as *climate feedbacks*, but since we here are dealing with precipitation they are simply a set of terms within the atmospheric budget. The precipitation response $\Delta P$ can be divided into contributions from the RA and post-eruption SST cooling ($\Delta P_{RA}$ and $\Delta P_{SST}$). $\Delta P_{RA}$ is commonly referred to as the precipitation *fast response* while $\Delta P_{SST}$ is the precipitation *slow response*, with these terms conveying the longer timescales of sea surface temperature adjustment than for the atmosphere and land alone (Andrews et al., 2010; Samset et al., 2016).

With this decomposition, the $\Delta R_{ATM}$ term in Equation 1 breaks down into the atmospheric aerosol forcing, $\Delta R_{ATM,IRF}$, plus the radiative responses $\Delta R_{ATM,RA}$ and $\Delta R_{ATM,SST}$. We combine radiative and sensible heat flux terms into a diabatic cooling rapid adjustment and diabatic cooling SST-mediated response, $\Delta Q_{RA}$ and $\Delta Q_{SST}$. Decomposing Equation 1 in this way yields:

$$\underbrace{L\Delta P_{RA} + L\Delta P_{SST}}_{L\Delta P} \approx \underbrace{-\Delta R_{ATM,IRF}}_{forcing \times -1} \underbrace{-(\Delta R_{ATM,RA} + \Delta SH_{RA})}_{+\Delta Q_{RA}} \underbrace{-(\Delta R_{ATM,SST} + \Delta SH_{SST})}_{+\Delta Q_{SST}} \quad (2)$$

In our post-eruption case, precipitation does not simply balance the atmospheric radiative forcing on its own, since precipitation in the troposphere cannot respond to stratospheric aerosols as readily as other components of the atmosphere's energy budget within $\Delta Q_{RA}$ and $\Delta Q_{SST}$. As we will show, some terms in Equation 2 balance $\Delta R_{ATM,IRF}$ while others add to its influence, with precipitation anomalies being among several covarying responses. To first order, we will interpret the precipitation response as balancing the remainder between the atmospheric aerosol forcing and faster-acting radiative and sensible heat responses.

By quantifying the various terms in Equation 2, we here identify the key mechanisms that result in post-eruption precipitation reduction. While similar analyses of the atmospheric energy budget have been performed for anthropogenic tropospheric aerosol and greenhouse gas impacts (Andrews et al., 2010; Previdi, 2010; Samset et al., 2016), this has not to the best of our knowledge been carried out for volcanic aerosols.

## 2. Methods

### 2.1. GISS ModelE2.2 Simulations

The main set of simulations we examine here were produced by DallaSanta and Polvani (2022), who used the Goddard Institute for Space Studies (GISS) ModelE2.2. ModelE2.2 is a "high-top" version of the NASA GISS ModelE Earth system model created to optimize stratospheric climate (Orbe et al., 2020), with 102 vertical levels in total and a model top at 0.002 hPa. Volcanic aerosol radiative impacts are generated according to refractive indices from Palmer and Williams (1975), assuming 75% sulfuric acid to 25% water by mass. Among several tropical eruption cases generated for DallaSanta and Polvani (2022), we analyze the simulations of a 20 Tg sulfur (S) injection case. This represents a sulfur injection between the magnitudes of Mt. Pinatubo's 1991 eruption and the larger 1815 eruption of Mt. Tambora. We chose this sulfur mass to provide enough signal to dominate over precipitation's internal variability on large spatial scales.

We analyze two 20-member ensembles of ModelE2.2 runs: one ensemble with a fully coupled model configuration, where SSTs are capable of responding to the eruption, and another with a land-atmosphere only

configuration and prescribed SSTs unable to respond. We refer to these ensembles as *interactive SST* and *fixed SST* cases, respectively. For both ensembles, each member is branched off from a separate ENSO-neutral state of a long control run having pre-industrial forcings, with a tropical eruption occurring on the following June 15th. Volcanic aerosols are input as aerosol extinction and size values created with the Easy Volcanic Aerosol forcing generator (Toohey et al., 2016). In the fixed SST runs, the SSTs are taken from the corresponding years of the control run, wherein no eruption occurs. Subtracting values from the two ensembles, pairwise, isolates the role of SST-mediated responses (only present with interactive SSTs) from the direct atmospheric aerosol forcing and rapid adjustments. Subtracting values from the corresponding control runs defines the post-eruption response in each case, also referred to as the post-eruption anomaly. We also assess the spread across each 20-member ensemble to quantify the magnitude of internal variability. Volcanic aerosol radiative forcings (the IRF) are calculated online at each time step, using double radiation calls with and without factoring in the volcanic aerosols. For the atmospheric aerosol radiative forcings used in our analysis, we use the difference between top-of-atmosphere and surface IRFs calculated by the model in this way.

### 2.2. VolMIP Simulations

To assess the robustness of results from the GISS model, we supplement the above analysis with a multi-model evaluation of simulations from the Volcanic forcing Model Intercomparison Project (VolMIP) (Zanchettin et al., 2016). Here we assess the central VolMIP experiment, *volc-pinatubo*, which simulates the response to an idealized Pinatubo-like eruption by prescribing volcanic aerosol radiative forcings from the CMIP6 reconstruction of the actual event (Thomason et al., 2016). The five models we analyze are CanESM5, GISS ModelE2.1, MIROC-ES2L, MPI-ESM1.2-LR, and UKESM1. Here we analyze 25 simulations of each model, a number stipulated in the VolMIP protocol. We use output for the 2-year period beginning with the eruption, as this was the largest number of full post-eruption years available from all models. Note that this is shorter than the 4-year period we use our ModelE2.2 analysis, and that the GISS simulations in VolMIP are from a different model version (ModelE2.1) with fewer vertical levels (40) and a lower model top (0.01 hPa).

### 2.3. Radiative Kernel Analysis

We use radiative kernels to elucidate how volcanic aerosols influence precipitation by altering radiative fluxes. In the radiative kernel method, simulated changes to state variables are multiplied by kernels quantifying changes in radiative flux for a unit change in the variable at each location, altitude, and month-of-year (Soden et al., 2008). Kernel-derived temperature, water vapor, and surface albedo responses were calculated using the ClimKern analysis package (Janoski & Mitevski, 2023). To quantify the atmospheric radiative responses that drive precipitation change, we subtracted kernels of surface responses from those representing top-of-atmosphere responses (Previdi, 2010).

We primarily use the CloudSat radiative kernels (Kramer et al., 2019), which are based on satellite observations. To confirm that our key results are not kernel dependent, in our VolMIP analysis we additionally use kernels derived from the GFDL (Soden et al., 2008) and ECHAM6 (Block & Mauritsen, 2013) models. In our analyses, we separate the atmospheric temperature response above and below 200 hPa, based on the approximate boundary between aerosol-induced warming above and cooling below that level, to distinguish the impacts of these temperature responses. Cloud responses are not directly calculated by these kernels, yet can be estimated as a remainder. Since the VolMIP models did not output aerosol IRFs, we here treat the difference between simulated radiative flux anomalies and all kernel-derived responses as a combined atmospheric "aerosol forcing + cloud response."

## 3. Results

### 3.1. Linking Post-Eruption Precipitation Reduction to the Atmosphere's Energy Balance

We first examine post-eruption global precipitation reduction in our model, establish the extent to which it is associated with fast and slow responses, and verify that diabatic cooling is a useful indicator of the precipitation response to volcanic aerosols. We start by presenting the decline in global mean precipitation in the GISS ModelE2.2 simulations of a 20 Tg S eruption. As seen in Figure 1a, within 3 months of the simulated eruptions, global mean precipitation is reduced. This is true not only for the ensemble mean (solid black line), but for all ensemble members (gray area). This decline in global precipitation is sustained for several years in the ensemble

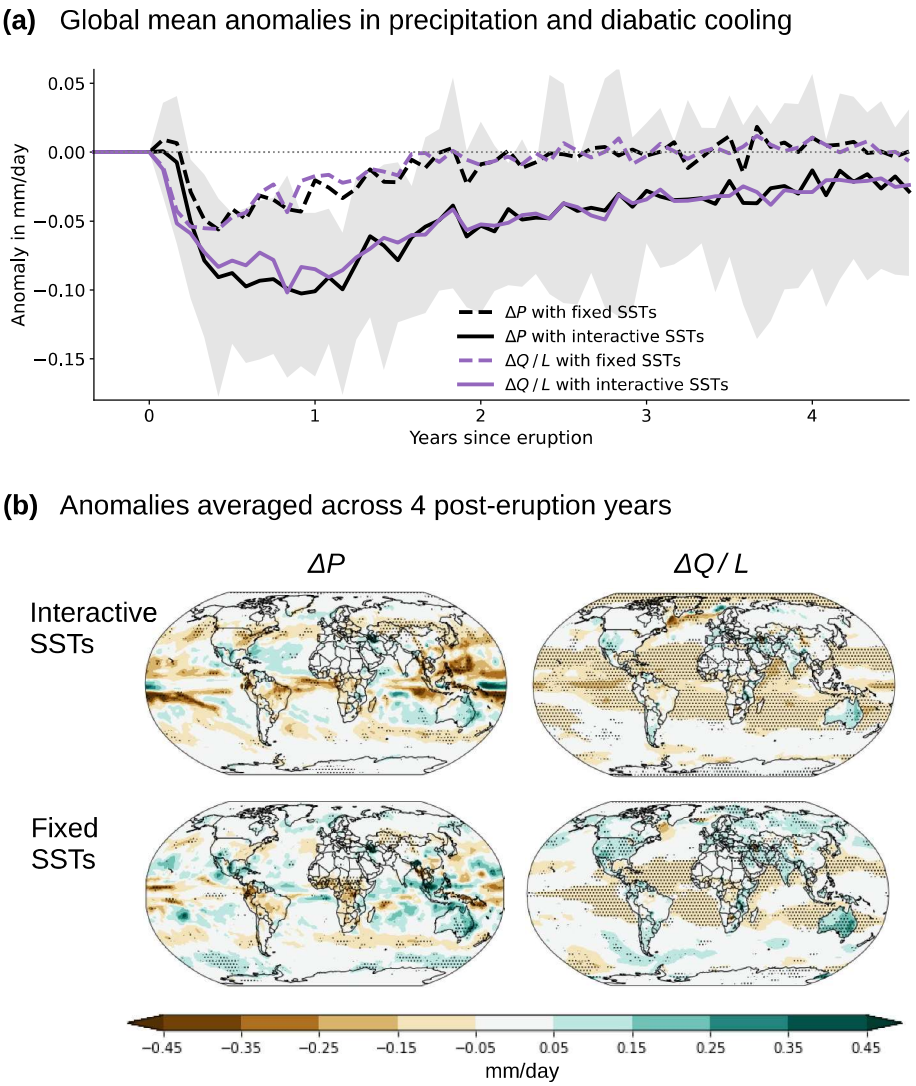


**Figure 1.** Post-eruption global precipitation reduction in GISS ModelE2.2 experiments. (a) Time series of precipitation anomalies averaged across the ensemble of 20 Tg S eruptions and (b) maps of anomalies averaged over the 4 years following the eruption. In (a), precipitation anomalies are shown alongside the concurrent diabatic cooling (divided by $L$ to be in precipitation units). Shading in (a) denotes the full spread across the interactive SST ensemble, while stippling in (b) denotes agreement in sign among at least 80% of members in the presented ensemble.

mean, and for one and a half years in every ensemble member. The ensemble mean decline in precipitation over the four post-eruption years amounts to a 2% reduction, with 4% reduction during the month of maximum response, nearly 1 year after the eruption.

We next consider the precipitation in the fixed SST ensemble in order to disentangle the roles of the fast and slow responses. Both the fast precipitation response (dashed black line) and slow response (difference between solid and dashed black lines) are revealed to be important. However, the fast response on average lasts slightly less than 2 years, due to its dependence on the presence of volcanic aerosols. In contrast, the slow response—which becomes the largest precipitation driver after the first 6 months—lasts for several years: this reflects the far longer time scale for the ocean to equilibrate compared to the atmosphere.

We now demonstrate that post-eruption precipitation anomalies closely balance diabatic cooling from the sum of radiative and sensible heat flux anomalies, which we convert into precipitation-equivalent units ($\Delta Q/L$) and plot in Figure 1a. Comparing the purple $\Delta Q/L$ lines of Figure 1a to the black $\Delta P$ lines, it is clear that this

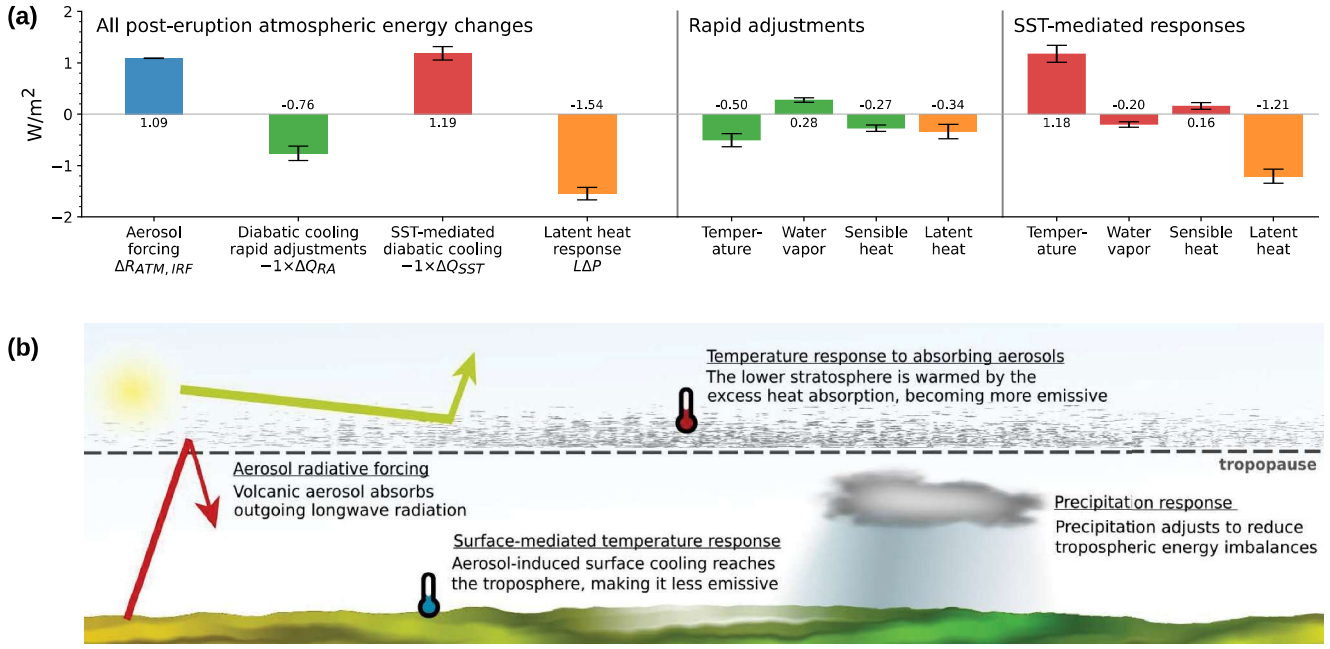


**Figure 2.** Atmospheric energetic perturbations after a volcanic eruption in GISS ModelE2.2 experiments. In (a) each bar shows the ensemble mean quantified over the 4-year period beginning with the month of the eruption, while uncertainties denote ±1 standard deviation among ensemble members. In (b) we visualize the dominant perturbations. All terms in (a) are represented with the sign convention of positive anomalies denoting increased net energy flux into the atmosphere. Positive radiative and sensible terms hence convey reduced diabatic cooling.

diabatic cooling closely approximates post-eruption precipitation anomalies on a global scale. While this is well-known in model experiments with sustained forcings (Dagan et al., 2021; O'Gorman et al., 2012), the relationship has not to our knowledge been shown for transient forcings such as tropical eruptions. The precipitation response's lag behind diabatic cooling in the first post-eruption months (see the two solid lines) reflects the duration the atmosphere takes to fully adjust to a stratospheric forcing, but no substantial difference persists after the first year. These results confirm that diabatic cooling is a useful indicator of post-eruption precipitation response.

### 3.2. Connection to Regional Precipitation Responses

On regional scales (Figure 1b), one sees a weaker relationship between diabatic cooling and precipitation than on global average, as the energy transport $\Delta H$ constituting their difference becomes important. Contrasting the left and right panels in Figure 1b, we see that $\Delta H$ sharpens differences in precipitation response across regions, and enhances the spread across ensemble members. Even for this large eruption case, precipitation responses lack robustness across ensemble members at nearly every location. This is evident in the lack of locations with at least 80% of agreement in sign among ensemble members (stippling in the $\Delta P$ maps of Figure 1b). While regional responses to volcanic aerosols are complex, one can see that diabatic cooling remains important and governs the response at the largest regional scales, with $\Delta H$ redistributing these anomalies across locations.

It is apparent from Figure 1b that land regions show a smaller post-eruption $\Delta Q$ response than over the oceans, yet tropical Africa and South America, Southeast Asia, and Eastern North America nonetheless evidence relatively strong precipitation reductions. These regions are all wetter than their surroundings (Adler et al., 2018), following a "wet gets drier" post-eruption pattern (Iles et al., 2013) that is opposite the one in response to greenhouse gases (Held & Soden, 2006). In energy budget analyses, the pattern reflects the *thermodynamic* component of $\Delta H$ (Muller & O'Gorman, 2011). Though we do not here separately compute thermodynamic and dynamical $\Delta H$ contributions, both can play a role in shaping regional responses. The muted $\Delta Q$ response over continents reflects sensible heat rapid adjustments (see Figure S1 in Supporting

Information S1), which act to negate atmospheric radiative responses specifically over land as occurs for other forcings (Myhre et al., 2018).

### 3.3. Mechanisms of the Global Post-Eruption Precipitation Response

We now decompose the post-eruption diabatic cooling responses in ModelE2.2 to deduce the mechanisms driving global precipitation reduction. In the left panel of Figure 2a, we plot the four components of the energy balance as grouped by the curly brackets below Equation 2, with the terms reordered to highlight the causality sequence from atmospheric aerosol forcing to resulting precipitation response. The volcanic aerosols add energy directly into the atmosphere via absorption of longwave radiation. This and aerosol-induced solar reflection drive rapid adjustments and SST-mediated responses in both radiative and sensible heat, along with latent heat responses from the resulting precipitation changes. These four terms in the left panel closely balance each other, summing to a negligible $-0.006$ W/m$^2$. Note that the volcanic aerosol forcing and SST-mediated diabatic cooling response both bring energy into the atmosphere, whereas the rapid adjustments and precipitation (latent heat) reduction remove energy to restore equilibrium.

In the middle and right panels of Figure 2a, we show the dominant terms in the rapid adjustments and SST-mediated responses. In these panels, the radiative term $\Delta R_{ATM}$ is decomposed using the CloudSat radiative kernels (see Section 2), from which we show only the temperature and water vapor responses that dominate the signal. The water vapor and sensible heat terms closely cancel each other. We will hence focus on the atmospheric aerosol forcing, the temperature rapid adjustment, and the SST-mediated temperature response as key to understanding the global precipitation response to volcanic aerosols. We note that the fixed SST simulations reveal $-0.26$ W/m$^2$ of rapid adjustments not attributed by the kernels to evaluated adjustments. This may reflect cloud radiative responses similar to those identified for responses to $CO_2$ (Kamae et al., 2015), though we lack sufficient model output (particularly clear-sky IRFs) to isolate cloud responses.

We now identify the mechanisms driving the precipitation fast response. Absorption of outgoing longwave radiation by volcanic aerosols adds a flux of energy into the stratosphere that dominates the atmospheric aerosol forcing shown in Figure 2a. Shortwave effects reduce the flux 35% compared to the longwave IRF alone. Note that unlike the more frequently studied top-of-atmosphere aerosol forcing, where shortwave reflection dominates, the atmospheric aerosol forcing consists of a smaller shortwave effect wherein reflection prevents light from reaching underlying shortwave absorbers (e.g., water vapor and black carbon). These differences are apparent when decomposing longwave and shortwave responses for both atmospheric and top-of-atmosphere fluxes (see Figure S2 in Supporting Information S1).

Because the added energy flux is primarily colocated with the aerosols in the stratosphere, it cannot be readily balanced by a latent heat response in the underlying troposphere. The surplus energy hence causes the air surrounding the aerosol layer to warm, as shown in the left panel of Figure 3a. This in turn enhances the emissivity of the atmosphere above ~200 hPa via Planck's law, which partly cancels the surplus energy flux. This emissivity response is shown as the green line in Figure 3b, and dominates the diabatic cooling rapid adjustment (see Figure 2a). Increased emission out of the atmosphere due to stratospheric warming weakens the precipitation reduction by curtailing the energetic need for latent heat changes to restore equilibrium (compare terms in Figure 2a, noting that the latent heat rapid adjustment is equal to the 4-year average of precipitation with fixed SSTs in Figure 1, scaled by $L$). That precipitation can respond to an energetic imbalance centered in the overlying stratosphere is driven by increased stratosphere-to-troposphere flux of longwave radiation, which thermodynamically inhibits precipitation when the excess flux is absorbed by clouds or co-located greenhouse gases. As deduced from stratospheric aerosol injection experiments (Ferraro et al., 2014), this downward flux enhancement stems not only from reemission of absorbed longwave radiation but also through stratospheric warming strengthening downward emission, which we note could partly offset the above-described mechanism whereby stratospheric warming weakens precipitation decline.

We next identify the mechanisms driving the slow precipitation response that, we recall, is an indirect response resulting from the reflection of incoming sunlight away from Earth's surface by volcanic aerosols. This reflection alters the atmospheric energy budget primarily by cooling the surface due to it being less insolated than before the eruption. Because tropospheric temperature is largely controlled by the underlying surface, the surface cooling in turn cools the troposphere (see the right panel of Figure 3a). The tropospheric temperature anomaly is overall stronger than at surface, as occurs in response to greenhouse gases (Manabe & Wetherald, 1975; Santer

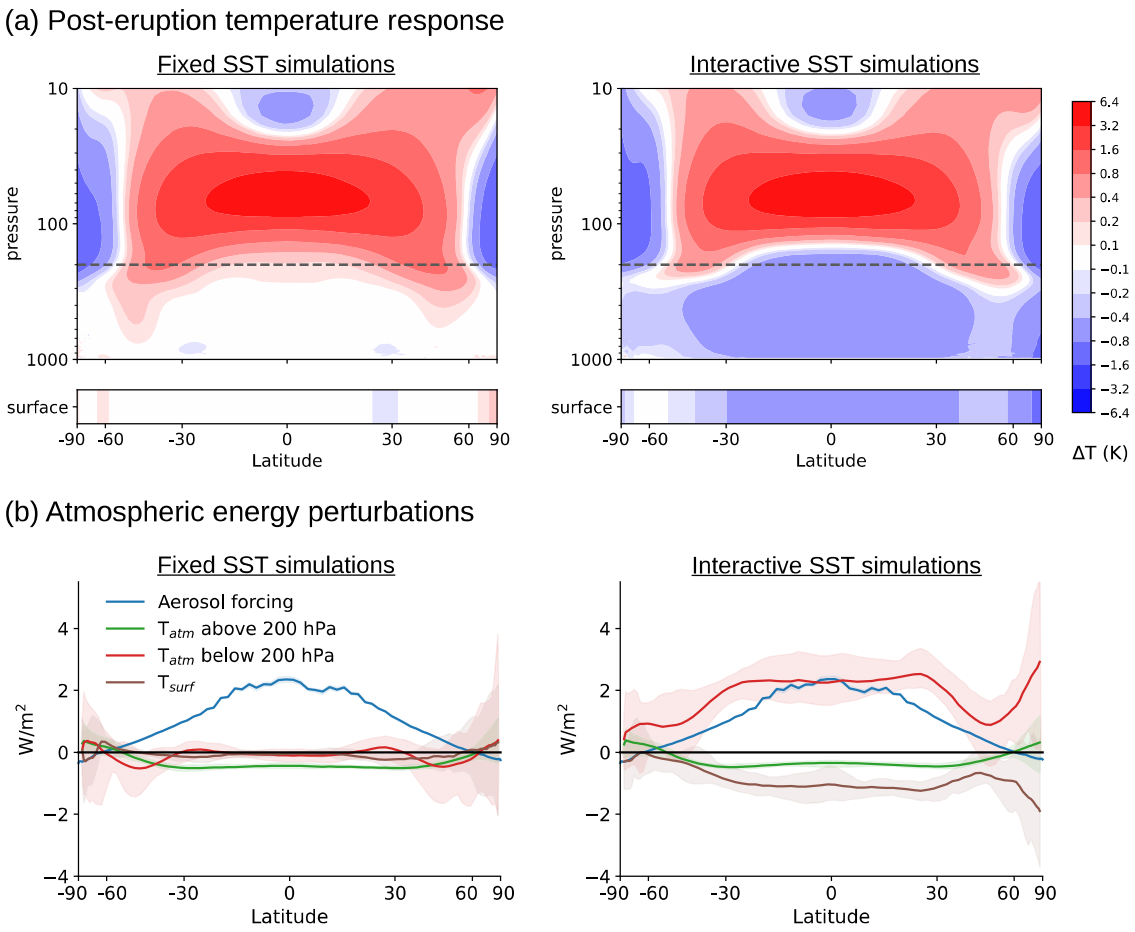


**Figure 3.** Post-eruption (a) temperature changes and (b) the associated kernel-derived atmospheric energy responses. In (b), we also include the atmospheric aerosol forcing calculated by the model. Results shown are ensemble means averaged over the four post-eruption years. Shading in (b) denotes the full spread among ensemble members, and solid lines represent ensemble means.

et al., 2005). Likewise, the decreased emissivity of the atmosphere due to tropospheric cooling overpowers the decreased emissivity of the surface into the troposphere due to surface cooling (compare red and brown lines, respectively, in the right panel of Figure 3b). The SST-mediated temperature response overall brings energy into the troposphere, which drives a closely balancing global precipitation reduction (compare SST-mediated temperature and latent heat responses in Figure 2a). Hence, much of the global precipitation reduction over the assessed 4-year period is an indirect influence of aerosol-induced surface cooling rather than a direct influence of the aerosol's radiative influence on the atmospheric energy balance. In Figure 2b, we illustrate the four dominant global atmospheric energy terms discussed above.

### 3.4. Model Spread in Post-Eruption Atmospheric Energy Budget Responses

We next analyze the VolMIP models, to confirm that the identified mechanisms leading to post-eruption precipitation response are robust across climate models and radiative kernels. Our results are presented in Figure 4, where different colors show different models, and different symbols show different kernels. We note some methodological differences from the previous section. The VolMIP output analyzed here is for the 7–9 Tg S injection from Mt. Pinatubo, not a 20 Tg S idealized eruption. Further, we cannot separate rapid adjustments from SST-mediated responses here, because all VolMIP simulations use interactive SSTs.

Nonetheless, as one can see in Figure 4, the VolMIP models confirm the results of the previous section. First, all combinations of models and kernels show that temperature anomalies above 200 hPa remove energy from the atmosphere, with remaining temperature responses adding energy. Second, the VolMIP models show that water

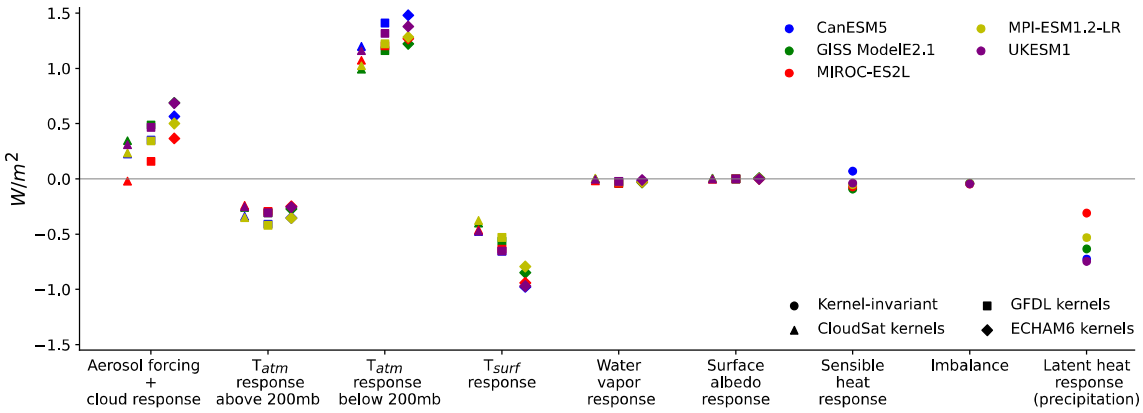


**Figure 4.** Post-eruption intermodel spread across VolMIP, for ensemble means of five climate models simulating a Pinatubo-like eruption. We repeat this analysis using three sets of radiative kernels. Each color represents a different model, while each symbol represents a different kernel.

vapor, surface albedo, and sensible heat responses are all too minor to substantially influence global precipitation change. Third, the VolMIP models confirm that combining latent, sensible, and radiative flux terms leaves a negligible energy imbalance, validating our methodology.

Not enough output is provided by VolMIP to separate atmospheric aerosol forcings from cloud responses, yet we anticipate that cloud responses dominate the model spread. Our rationale for expecting the aerosol forcings to be robust is that all the models prescribe the same volcanic aerosol scenario in VolMIP, and models tend to use identical volcanic aerosol optical properties (Palmer & Williams, 1975). Further study is needed to quantify the influence of cloud responses on post-eruption precipitation response and its intermodel spread.

## 4. Conclusions

We have shown that global post-eruption precipitation reduction largely—but not solely—stems from tropospheric cooling due to volcanic aerosols blocking incoming sunlight. As the assessed simulations revealed, this mechanism is mediated by cooler post-eruption SSTs. Absorption of outgoing longwave radiation by volcanic aerosols further reduces precipitation, and is the dominant cause of precipitation decline in the first few post-eruption months, until the SST-mediated response overpowers it. These mechanisms are robust across climate models and radiative kernels.

We identify three caveats of our analysis that future evaluations may want to improve upon. First, our quantifications of cause and effect are simplified in that precipitation changes could drive radiative and sensible flux responses rather than solely vice-versa. Second, we were unable to isolate the role of cloud radiative responses, which our results suggest affect the magnitude of post-eruption precipitation reduction and generate intermodel disagreement. And third, we relied wholly on models without seeking observational signatures of the precipitation decline's mechanisms.

The methods applied here could be useful for better understanding and predicting precipitation responses to stratospheric aerosols. We found that precipitation responses are intricately tied to stratospheric aerosols' reflective and absorptive characteristics across wavelengths. Aerosols of different physical properties—for example, mass, size, or composition—can hence affect precipitation dissimilarly. Connecting aerosol properties to precipitation responses through the energy budget could improve constraints on large-scale responses to other volcanic scenarios, as well as stratospheric aerosol geoengineering and wildfire smoke cases. Similarly, regional impacts could be elucidated through further evaluation of atmospheric energy transport and its response to aerosols.

## Data Availability Statement

ModelE source code is available online (NASA GISS, 2023), and simulation output used here is on a Zenodo archive (McGraw et al., 2023). VolMIP data is available online at the CMIP6 repository (Program for Climate Model Diagnosis & Intercomparison, 2023).

**Acknowledgments**
The authors thank Kevin DallaSanta for clarifications on the GISS ModelE2.2 simulations, which he had generated for a previous study. We also thank Dana Raiter and Ryan Kramer for useful discussions. This work was funded by the US National Science Foundation through award 2303352 to Columbia University.

## References

Adler, R. F., Sapiano, M. R. P., Huffman, G. J., Wang, J.-J., Gu, G., Bolvin, D., et al. (2018). The global precipitation climatology project (GPCP) monthly analysis (new version 2.3) and a review of 2017 global precipitation. *Atmosphere*, *9*(4), 138. https://doi.org/10.3390/atmos9040138

Andrews, T., Forster, P. M., Boucher, O., Bellouin, N., & Jones, A. (2010). Precipitation, radiative forcing and global temperature change. *Geophysical Research Letters*, *37*(14), L14701. https://doi.org/10.1029/2010GL043991

Block, K., & Mauritsen, T. (2013). Forcing and feedback in the MPI-ESM-LR coupled model under abruptly quadrupled $CO_2$. *Journal of Advances in Modeling Earth Systems*, *5*(4), 676–691. https://doi.org/10.1002/jame.20041

Colose, C. M., LeGrande, A. N., & Vuille, M. (2016). Hemispherically asymmetric volcanic forcing of tropical hydroclimate during the last millennium. *Earth System Dynamics*, *7*(3), 681–696. https://doi.org/10.5194/esd-7-681-2016

Dagan, G., & Stier, P. (2020). Constraint on precipitation response to climate change by combination of atmospheric energy and water budgets. *Npj Climate and Atmospheric Science*, *3*(1), 1–5. https://doi.org/10.1038/s41612-020-00137-8

Dagan, G., Stier, P., & Watson-Parris, D. (2021). An energetic view on the geographical dependence of the fast aerosol radiative effects on precipitation. *Journal of Geophysical Research: Atmospheres*, *126*(9), e2020JD033045. https://doi.org/10.1029/2020JD033045

DallaSanta, K., & Polvani, L. M. (2022). Volcanic stratospheric injections up to 160 Tg(S) yield a Eurasian winter warming indistinguishable from internal variability. *Atmospheric Chemistry and Physics Discussions*, 1–31. https://doi.org/10.5194/acp-2022-58

Ferraro, A. J., Highwood, E. J., & Charlton-Perez, A. J. (2014). Weakened tropical circulation and reduced precipitation in response to geoengineering. *Environmental Research Letters*, *9*(1), 014001. https://doi.org/10.1088/1748-9326/9/1/014001

Gillett, N. P., Weaver, A. J., Zwiers, F. W., & Wehner, M. F. (2004). Detection of volcanic influence on global precipitation. *Geophysical Research Letters*, *31*(12), L12217. https://doi.org/10.1029/2004GL020044

Held, I. M., & Soden, B. J. (2006). Robust responses of the hydrological cycle to global warming. *Journal of Climate*, *19*(21), 5686–5699. https://doi.org/10.1175/JCLI3990.1

Iles, C. E., & Hegerl, G. C. (2014). The global precipitation response to volcanic eruptions in the CMIP5 models. *Environmental Research Letters*, *9*(10), 104012. https://doi.org/10.1088/1748-9326/9/10/104012

Iles, C. E., Hegerl, G. C., Schurer, A. P., & Zhang, X. (2013). The effect of volcanic eruptions on global precipitation. *Journal of Geophysical Research: Atmospheres*, *118*(16), 8770–8786. https://doi.org/10.1002/jgrd.50678

Janoski, T. P., & Mitevski, I. (2023). ClimKern (version 1.0.0) [Software]. https://doi.org/10.5281/zenodo.10291284

Kamae, Y., Watanabe, M., Ogura, T., Yoshimori, M., & Shiogama, H. (2015). Rapid adjustments of cloud and hydrological cycle to increasing $CO_2$: A review. *Current Climate Change Reports*, *1*(2), 103–113. https://doi.org/10.1007/s40641-015-0007-5

Kramer, R. J., Matus, A. V., Soden, B. J., & L'Ecuyer, T. S. (2019). Observation-based radiative kernels from CloudSat/CALIPSO. *Journal of Geophysical Research: Atmospheres*, *124*(10), 5431–5444. https://doi.org/10.1029/2018JD029021

Liu, F., Chai, J., Wang, B., Liu, J., Zhang, X., & Wang, Z. (2016). Global monsoon precipitation responses to large volcanic eruptions. *Scientific Reports*, *6*(1), 24331. https://doi.org/10.1038/srep24331

Manabe, S., & Wetherald, R. T. (1975). The effects of doubling the $CO_2$ concentration on the climate of a general circulation model. *Journal of the Atmospheric Sciences*, *32*(1), 3–15. https://doi.org/10.1175/1520-0469(1975)032<0003:TEODTC>2.0.CO;2

McGraw, Z., DallaSanta, K., & Polvani, L. M. (2023). ModelE2.2 output used in "How volcanic aerosols globally inhibit precipitation" study [Dataset]. *Zenodo*. https://doi.org/10.5281/zenodo.10407931

Muller, C. J., & O'Gorman, P. A. (2011). An energetic perspective on the regional response of precipitation to climate change. *Nature Climate Change*, *1*(5), 266–271. https://doi.org/10.1038/nclimate1169

Myhre, G., Samset, B. H., Hodnebrog, Ø., Andrews, T., Boucher, O., Faluvegi, G., et al. (2018). Sensible heat has significantly affected the global hydrological cycle over the historical period. *Nature Communications*, *9*(1), 1922. https://doi.org/10.1038/s41467-018-04307-4

NASA GISS. (2023). GISS GCM ModelE [Software]. Retrieved from https://www.giss.nasa.gov/tools/modelE/

O'Gorman, P. A., Allan, R. P., Byrne, M. P., & Previdi, M. (2012). Energetic constraints on precipitation under climate change. *Surveys in Geophysics*, *33*(3), 585–608. https://doi.org/10.1007/s10712-011-9159-6

Orbe, C., Rind, D., Jonas, J., Nazarenko, L., Faluvegi, G., Murray, L. T., et al. (2020). GISS model E2.2: A climate model optimized for the middle atmosphere—2. Validation of large-scale transport and evaluation of climate response. *Journal of Geophysical Research: Atmospheres*, *125*(24), e2020JD033151. https://doi.org/10.1029/2020JD033151

Palmer, K. F., & Williams, D. (1975). Optical constants of sulfuric acid; application to the clouds of Venus? *Applied Optics*, *14*(1), 208–219. https://doi.org/10.1364/AO.14.000208

Previdi, M. (2010). Radiative feedbacks on global precipitation. *Environmental Research Letters*, *5*(2), 025211. https://doi.org/10.1088/1748-9326/5/2/025211

Proctor, J., Hsiang, S., Burney, J., Burke, M., & Schlenker, W. (2018). Estimating global agricultural effects of geoengineering using volcanic eruptions. *Nature*, *560*(7719), 480–483. https://doi.org/10.1038/s41586-018-0417-3

Program for Climate Model Diagnosis & Intercomparison. (2023). Archive for climate model intercomparison project phase 6 [Dataset]. Retrieved from https://pcmdi.llnl.gov/CMIP6/

Robock, A., & Liu, Y. (1994). The volcanic signal in Goddard Institute for Space Studies three-dimensional model simulations. *Journal of Climate*, *7*(1), 44–55. https://doi.org/10.1175/1520-0442(1994)007<0044:TVSIGI>2.0.CO;2

Samset, B. H., Myhre, G., Forster, P. M., Hodnebrog, Ø., Andrews, T., Faluvegi, G., et al. (2016). Fast and slow precipitation responses to individual climate forcers: A PDRMIP multimodel study. *Geophysical Research Letters*, *43*(6), 2782–2791. https://doi.org/10.1002/2016GL068064

Santer, B. D., Wigley, T. M. L., Mears, C., Wentz, F. J., Klein, S. A., Seidel, D. J., et al. (2005). Amplification of surface temperature trends and variability in the tropical atmosphere. *Science*, *309*(5740), 1551–1556. https://doi.org/10.1126/science.1114867

Soden, B. J., Held, I. M., Colman, R., Shell, K. M., Kiehl, J. T., & Shields, C. A. (2008). Quantifying climate feedbacks using radiative kernels. *Journal of Climate*, *21*(14), 3504–3520. https://doi.org/10.1175/2007JCLI2110.1

Thomason, L. V., Vernier, J.-P., Bourassa, A., Arfeuille, F., Bingen, C., Peter, T., & Luo, B. (2016). Stratospheric aerosol data set (SADS version 2) prospectus. Retrieved from https://www.wcrp-climate.org/images/modelling/WGCM/CMIP/CMIP6Forcings_StratosphericAerosolDataSet_InitialDescription_150131.pdf

Toohey, M., Stevens, B., Schmidt, H., & Timmreck, C. (2016). Easy volcanic aerosol (EVA v1.0): An idealized forcing generator for climate simulations. *Geoscientific Model Development*, *9*(11), 4049–4070. https://doi.org/10.5194/gmd-9-4049-2016

Trenberth, K. E., & Dai, A. (2007). Effects of Mount Pinatubo volcanic eruption on the hydrological cycle as an analog of geoengineering. *Geophysical Research Letters*, *34*(15), L15702. https://doi.org/10.1029/2007GL030524

Zanchettin, D., Khodri, M., Timmreck, C., Toohey, M., Schmidt, A., Gerber, E. P., et al. (2016). The model intercomparison project on the climatic response to volcanic forcing (VolMIP): Experimental design and forcing input data for CMIP6. *Geoscientific Model Development*, *9*(8), 2701–2719. https://doi.org/10.5194/gmd-9-2701-2016

Zhuo, Z., Gao, C., Kirchner, I., & Cubasch, U. (2020). Impact of volcanic aerosols on the hydrology of the Asian monsoon and westerlies-dominated subregions: Comparison of proxy and multimodel ensemble means. *Journal of Geophysical Research: Atmospheres*, *125*(18), e2020JD032831. https://doi.org/10.1029/2020JD032831